Proceedings of the 21st ICSMGE, Vienna, Austria, 14 – 19 June 2026. Pistrol, Adam & Schweiger (eds.)
Published by: ÖGG, Austrian Society for Geomechanics, Salzburg, Austria, ISBN 978-3-9503898-4-5
https://doi.org/10.53243/ICSMGE2026-391

On the link between the contact fabric tensor and the intergranular strain tensor

Zekeriya Metehan Karslioglu, Sebastian Ullmann, Selma Schmidt, Ivo Herle
Institute of Geotechnical Engineering, TU Dresden, Germany, zekeriya_metehan.karslioglu@tu-dresden.de

ABSTRACT: Several constitutive models include the soil fabric as a state variable since it has been acknowledged that the fabric of a soil specimen can significantly influence the soil behavior. However, the initial values of these state variables are oftentimes only assumed as it is difficult to measure those in experiments. In this work, the possibilities to define the initial intergranular strain tensor, used in the extended hypoplastic model, from the contact fabric tensor of a soil specimen are explored. The approach is assessed by comparing the influence of the two tensors on the directional stiffness and the volumetric behavior of a soil in either element tests or DEM simulations.

KEYWORDS: Contact fabric, Intergranular strain, DEM, Element tests

1 INTRODUCTION

It has been known for several decades that the behavior of a soil specimen is dependent on the configuration of the grains and their contacts, i.e. the fabric of the soil. The influence of the initial fabric on the macroscopic soil behavior has already been studied 50 years ago by Oda (1972). With the help of more advanced tools emerging in the past decades, such as microfocus x-ray CT (μCT), researchers are now able to study not only the macroscopic evolution of soil specimens but also microscopic changes, which are also dependent on the initial fabric (e.g. Pinzón et al. 2023).

There are several constitutive models containing state variables somehow linked with the soil fabric, but the initial values of these state variables are generally only assumed and do not have any obvious link to the actual initial fabric of a soil specimen. In this work, the possibilities to calibrate the initial values of such a state variable from a given initial fabric are explored. More specifically, the hypoplastic model by von Wolffersdorff (1996) with the intergranular strains extension (Niemunis & Herle, 1997) is chosen as it is widely known and used.

The idea of the intergranular strain is, as the name suggests, based on the deformation at the grain interface or contact. It is therefore explored, if the initial value of the intergranular strain tensor can be calibrated from the initial contact fabric tensor, i.e. the initial configuration of the grain contacts. This is done by considering the directional stiffness of a soil element: In the intergranular strain concept, when a soil element is loaded, a higher stiffness can be achieved when the grain interface has been previously fully deformed in the opposite direction to the loading. On the other hand, when the grain interface is already fully deformed in the direction of loading, a lower stiffness is obtained. Considering the contact fabric of a soil element, a higher stiffness occurs in the direction in which most contact normals are oriented and a lower stiffness in the direction in which least contact normals are located. This directional dependency can also be observed in the volumetric behavior of the soil.

In this work, the Discrete Element Method (DEM) is used to generate two very different initial fabrics, one isotropic and one anisotropic, and to investigate their influence on the directional stiffness of a soil element. The initial intergranular strain tensors are then derived from the initial contact fabric tensors of the DEM specimens and their influence on the directional stiffness is again investigated in element test simulations. Hence, it can be assessed if the simulations with different initial intergranular strain tensors qualitatively influence the directional stiffness in the same manner as the different initial contact fabric tensors in the DEM simulations. Furthermore, it is also examined, whether the volumetric behavior resulting from different fabrics can be captured and correctly represented by the intergranular strain concept.

2 SOIL FABRIC

Soil fabric describes how particles and their contacts are arranged and oriented within the soil. This fabric develops through natural processes such as deposition, compaction, and loading, as well as during sample preparation in the laboratory. It captures important features of the internal soil structure that directly influence its behavior at the larger scale.

In this study, the focus is on the contact fabric, which refers to the network created by grain-to-grain contacts. Accordingly, the term fabric is mainly used to describe the orientations of these contact normals throughout the paper. To describe the contact fabric, two common features can be considered: contact density and the spatial distribution of contact normals. The density can be defined by the coordination number *CN*, which represent the average number of grain contacts per grain:

$$CN = 2 \cdot \frac{N_c}{N_p} \tag{1}$$

with N_c and N_p being the total number of contacts and grains, respectively. The spatial distribution can be represented as a second order fabric tensor **N** (Kanatani, 1984), which is defined as:

$$\mathbf{N} = \frac{1}{N}\sum_{i=1}^{N} \mathbf{n}_\mathrm{i} \otimes \mathbf{n}_\mathrm{i} \tag{2}$$

while $\mathbf{n}_\mathrm{i}$ denote the orientation vectors of the grain contacts and *N* the total number of grain contacts. An important aspect of the fabric tensor **N** is its anisotropy, which reflects how contact orientations deviate from a uniform distribution. This can be captured with the deviatoric fabric tensor **F**:

$$\mathbf{F} = \frac{15}{2}\left(\mathbf{N} - \frac{1}{3}\mathbf{I}\right) \tag{3}$$

with **I** being the identity tensor and the factor 15/2 the coefficient for the second order tensor. The anisotropy can be quantified with the anisotropy factor *a* (Gu et al. 2017):

$$a = \sqrt{\frac{3}{2}\mathbf{F} : \mathbf{F}} \tag{4}$$

The anisotropy influences the directional response of the soil under loading. When contacts are preferentially oriented in one direction, the soil tends to resist deformation more effectively along that direction. This leads to a directional dependence of the soil behavior that reflects the influence of the initial fabric.

To account for this within a continuum framework, the constitutive model must incorporate changes in stiffness that depend on the loading direction.

In this work, the extension of the hypoplastic model by von Wolffersdorff (1996) with the intergranular strains (Niemunis & Herle 1997) has been used to represent the effect of the initial fabric.

The intergranular strain extension was originally developed to capture the increase in stiffness observed after a reversal or change in the direction of deformation. It introduces an additional state variable, the so-called intergranular strain into hypoplasticity. This internal variable represents the material's directional memory and helps to prevent unrealistic accumulation of plastic strains during cyclic loading.

A change in stress can be described by the following general equation incorporating the material model stiffness **M** of the hypoplastic model:

$$\dot{\mathbf{T}} = \mathbf{M}(\mathbf{T}, \mathbf{D}, e, \boldsymbol{\delta}) : \mathbf{D} \tag{5}$$

Here, $\dot{\mathbf{T}}$ denotes the stress rate tensor. The matrix **M** depends on the stress state **T**, the stretching (or strain rate) tensor **D**, the void ratio e, and the intergranular strain tensor $\boldsymbol{\delta}$.

For the visual representation of constitutive equations, response envelopes, proposed by Gudehus (1979), serve as an effective graphical tool. These envelopes are shown as polar diagrams that depict the stress response in different strain rate directions, with greater distances from the origin indicating higher stiffness. The envelope's shape depends on the constitutive model and its state variables like the stress state and void ratio. These response envelopes are created by applying unit strain rates in various directions and calculating the corresponding stress responses predicted by the model for a specific current state.

Figure 1 shows the response envelopes simulated with the hypoplastic model, both with and without the intergranular strain extension. All cases start from the same initial isotropic stress state $\mathbf{T_0}$ and void ratio e, but differ in the initial intergranular strain tensor $\boldsymbol{\delta}$, which is fully aligned with the previous strain rate direction. Initially, the magnitude of the intergranular strain is at its maximum but with different directions of $\boldsymbol{\delta}$ ($\rho = ||\boldsymbol{\delta}||/R = 1$). The directions of these tensors are indicated by the arrows and are labeled as $\boldsymbol{\delta^A}$ and $\boldsymbol{\delta^B}$, with colors matching their respective response envelopes. The influence of the intergranular strain extension is reflected in the differences between the response envelopes. In the case, where the strain rate direction and the intergranular strain tensor face in the same direction ($\boldsymbol{\delta} : \mathbf{D} > 0$), the same behavior as the original hypoplasic model behavior is obtained. For the strain rate directions that differ from the direction of the intergranular strain ($\boldsymbol{\delta} : \mathbf{D} \leq 0$), the resulting stress increment is larger, indicating increased stiffness. This leads to a direction-dependent response envelope, where its size is scaled dependent on the alignment between the strain rate **D** and the intergranular strain tensor $\boldsymbol{\delta}$.

This highlights the importance of accurately defining the initial intergranular strain, due to its strong influence on direction-dependent variations in the incremental stiffness. To address this, a method is proposed to determine the initial intergranular strain tensor based on the material's initial fabric.

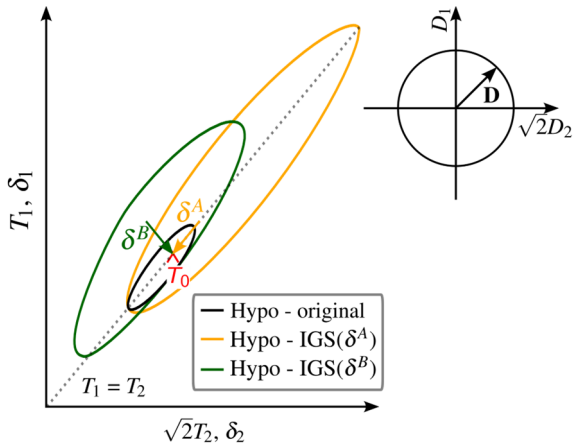

Figure 1. Response envelopes of the hypoplastic model, with and without intergranular strain, for different initial intergranular strain tensors at the same initial isotropic stress state $\mathbf{T_0}$ and void ratio e. The arrows shows the direction of the initial intergranular strain tensors $\boldsymbol{\delta^A}$ and $\boldsymbol{\delta^B}$. They are fully aligned with the previous strain rate **D** ($\rho = 1$).

The link to the fabric is made using the deviatoric fabric tensor **F**, which reflects the deviation of the orientations of contact normals from the isotropic state. Since the stiffness in the intergranular strain concept is dependent on the angle between the loading direction and the intergranular strain tensor, defining its initial state in alignment with the deviatoric fabric tensor **F** seems to be a meaningful representation of microscale anisotropy. To implement this, the initial intergranular strain tensor $\boldsymbol{\delta}$ is determined from a weighted fabric tensor **A**, which combines the identity tensor **I** and the deviatoric fabric tensor **F** according to the anisotropy factor a:

$$\mathbf{A} = \big(1 - \mathrm{f}(a)\big)\mathbf{I} + \mathrm{f}(a)\mathbf{F}, \qquad \boldsymbol{\delta} = \frac{\mathbf{A}}{||\mathbf{A}||} \cdot R \tag{6}$$

where the identity tensor **I** represents the perfectly isotropic state and the deviatoric fabric tensor **F** the anisotropic part. The relative weighting of these contributions is controlled by the anisotropy factor a through the exponential function

$$\mathrm{f}(a) = 1 - \mathrm{e}^{-a/c} \tag{7}$$

which varies between 0 and 1. The parameter c can be treated as a material parameter in this formulation. Small values of a give a stronger contribution from the identity tensor **I**, producing a state closer to isotropy, whereas larger a amplifies the influence of the deviatoric fabric tensor **F**, embedding the directional bias of the fabric into $\boldsymbol{\delta}$.

The orientation of $\boldsymbol{\delta}$ is aligned with that of the weighted fabric tensor **A**, while its magnitude is scaled by R, the hypoplastic model parameter representing the maximum length. This ensures that $\rho = ||\boldsymbol{\delta}||/R \leq 1$.

The procedure for the proposed method will be explained in detail with a representative example in the following sections.

3 GENERAL APPROACH

The proposed approach is evaluated through DEM and element test simulations. Two specimens with different initial fabrics (in DEM) or corresponding initial intergranular strain tensors (in element tests) are used to evaluate the incremental stiffness and the volumetric behavior. In the DEM simulations one sample is prepared by isotropic compression, the other by anisotropic compression.

For each specimen and method, strain-controlled loading up to 10 % strain is applied along one principal direction, either

vertical or horizontal, while stresses in the other two directions are maintained at -100 kPa, as illustrated in Figure 2. It should be noted that compression is considered negative and tension positive throughout this paper.

To determine the incremental stiffness, deviatoric stress and strain are used to isolate distortional (shape-changing) effects from volumetric changes. The incremental stiffness is calculated as:

$$G = \frac{\Delta q}{\Delta \varepsilon_q} \tag{8}$$

where Δq and $\Delta \varepsilon_q$ represent the increments in deviatoric stress and deviatoric strain, respectively. A deviatoric strain increment $\Delta \varepsilon_q$ of 0.1 % is chosen for the determination of the incremental stiffness.

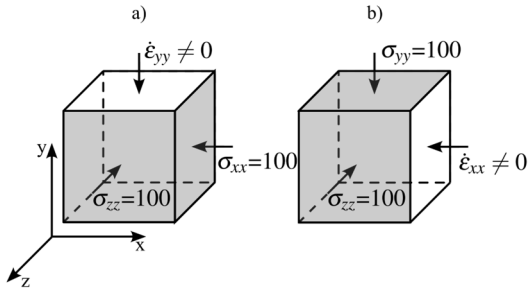

Figure 2. Boundary conditions of the strain-controlled loading tests: a) loading in vertical direction *y* and b) loading in horizontal direction *x* while the stresses in other directions were kept at -100 kPa.

4 DISCRETE ELEMENT SIMULATIONS

The influence of initial fabric anisotropy on directional stiffness was investigated by generating two granular assemblies using the DEM. To focus solely on the influence of fabric anisotropy, spherical particles were used to eliminate effects related to particle shape.

The simulations were carried out using the open-source DEM framework YADE (Smilauer et al. 2021). Particle interactions were governed by the Cundall–Strack contact law (Cundall & Strack 1979), which provides a physically meaningful representation of frictional contacts in granular media. To ensure numerical stability, the time step was set to 50 % of the estimated critical P-wave time step, as recommended in Smilauer et al. (2021). Simulations were performed without gravity, and a numerical damping coefficient of 0.2 was applied.

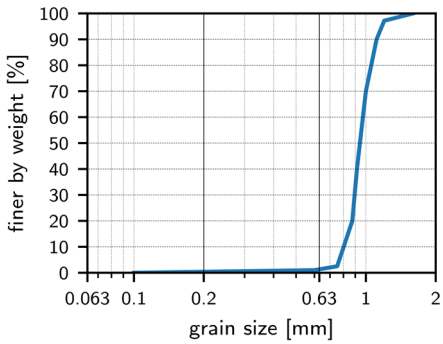

Figure 3. Grain size distribution of the DEM specimen.

The particles were modeled as linear-elastic frictional spheres, with a Young's modulus $E = 250$ MPa and a Poisson's ratio $\nu = 0.4$. Interparticle friction was defined by a microscopic internal friction angle $\varphi = 30°$. The assemblies were generated based on the grain size distribution of a coarse silica sand, as shown in Figure 3, with a median particle diameter $d_{50} = 0.943$ mm and a coefficient of uniformity $C_U = 1.2$.

The sample preparation method used follows a sequential process. First, a cloud of up to 20,000 spherical particles were generated randomly within a cuboidal space measuring 30 mm × 30 mm × 30 mm with no initial particle contacts. Periodic boundary conditions were applied in all three principal directions. Second, two distinct compression methods were employed to produce specimens with different initial fabrics while ensuring the same final confining pressure in all directions:

- **Isotropic compression:** Compression was applied simultaneously along all three directions (x, y, z) until an isotropic effective stress of 100 kPa was reached.
- **Anisotropic compression:** Compression was first applied vertically with zero horizontal (x, z) strains until $\sigma_{yy} = 100$ kPa. Then, horizontal compression followed while maintaining constant vertical stress, until $\sigma_{xx} = \sigma_{yy} = \sigma_{zz} = 100$ kPa.

In addition to the prescribed stress conditions, a threshold of 0.01 was set for the unbalanced force to define the end of the compression phase and to ensure that the specimens reached a quasi-static state before further testing. Due to this, stress fluctuations and temporary overshoots occurred during the iterative process.

Macroscopic properties such as the void ratio, along with microscopic measures including the coordination number, the fabric tensor, its deviatoric part, and the anisotropy factor, were used to describe the specimens prepared by the two compression methods. These parameters were determined from the DEM simulation data by analyzing particle interactions and arrangements using SPAM, a dedicated computational tool for spatial analysis (Stamati et al. 2020).

The state variables of the generated specimens are summarized in Table 1. Although the specimens underwent different stress paths during sample preparation, both methods resulted in similar void ratios and coordination numbers at the same mean (isotropic) effective stress p'.

Table 1. Mean effective (isotropic) stress p', void ratio e, coordination number CN and the scalar anisotropy factor a for the sample preparation methods.

State variables		isotropic	anisotropic
p'	[kPa]	-100	
e	[-]	0.642	0.640
CN	[-]	2.41	2.43
a	[-]	0.033	0.324

The scalar anisotropy factor a in Table 1 quantifies the microscale differences, approaching zero for isotropic states and increasing with directional bias. It is notably higher for the anisotropically compressed specimen. Figure 4 illustrates this with surface plots of the deviatoric fabric tensor **F**: the isotropic specimen shows a nearly spherical distribution, while the anisotropic specimen exhibits a vertically elongated shape, indicating strong fabric anisotropy.

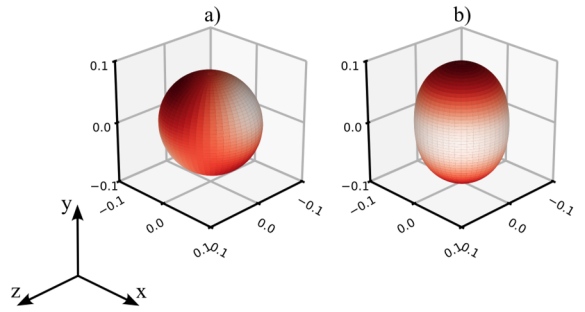

Figure 4. Surface plot of the distribution density of the deviatoric fabric tensor **F** for the sample prepared with a) isotropic compression and b) anisotropic compression.

These two specimens, prepared by isotropic and anisotropic compression, served as initial conditions for the strain-controlled tests described previously.

Figure 5 shows the stress–strain curves from DEM simulations, including a zoomed view of the initial 0.1 % deviatoric strain, which is used to determine the incremental stiffness. For the test with a vertically oriented fabric under vertical loading (A-0), the highest deviatoric stresses are observed and the peak stress is reached at the lowest shear strains. Under horizontal loading (A-90), which is perpendicular to the dominant fabric orientation, the response is softer and a more gradual rise to the peak stress can be acknowledged. The tests with isotropic fabric specimens exhibited similar behavior regardless of loading direction (I-0 and I-90), with stress levels between those of the tests A-0 and A-90. Notably, after about 8 % deviatoric strain ε_q, the deviatoric stresses q in all tests converge, indicating that the influence of the initial fabric decreases with continued loading.

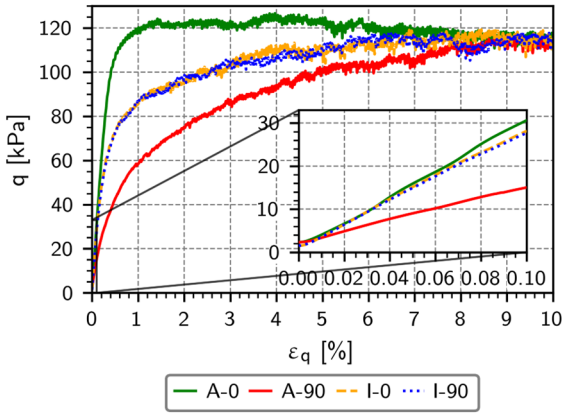

Figure 5. DEM: Stress-strain curves of the tests with different initial fabric configurations and loading conditions. Vertically oriented fabric under vertical (A-0) and horizontal (A-90) loading. Isotropic oriented fabric under vertical (I-0) and horizontal (I-90) loading.

The volumetric behavior of the tests is shown in Figure 6. All specimens initially exhibit contractive behavior, which then transitions into dilative behavior, typical for dense specimens. The observed differences in the volumetric responses of the specimens are closely linked to the stress-strain responses (Figure 5). The specimen that developed higher stress levels earlier (A-0) also exhibited a smaller contractancy and an earlier transition to dilatancy. This suggests a more stable fabric in that loading direction. In contrast, loading perpendicular to the dominant fabric orientation (A-90) results in a more pronounced contractancy, reflecting an open fabric in that loading direction. In this case, it also can be observed that dilatancy starts at higher deviatoric strains. The tests with isotropic specimens (I-0 and I-90) again showed intermediate behavior, consistent with their stress-strain curves.

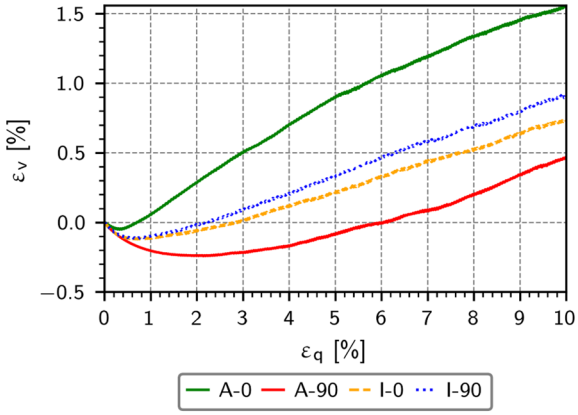

Figure 6. DEM: Volumetric strain curves of the tests with different initial fabric configurations and loading conditions.

5 ELEMENT TEST SIMULATIONS

The previously described strain-controlled loading tests were also simulated as element tests using the software Tochnog by Roddeman (2022). The model parameters were chosen based on typical values reported for sands in the literature and are summarized in Table 2. These parameters do not intend to represent the spherical particles used in the DEM simulations. Instead, they were used for a qualitative comparison of mechanical behavior based on the different initial intergranular strain tensors. The values of the initial state variables for the element test simulations are summarized in Table 3.

Table 2. Hypoplastic model parameters used for the element test simulations.

φ_c [°]	h_s [MPa]	n [-]	e_{i0} [-]	e_{c0} [-]	e_{d0} [-]	α [-]	β [-]
30	230	0.5	0.995	0.865	0.579	0.13	2.4

R [-]	m_R [-]	m_T [-]	β_r [-]	χ [-]
0.0001	5	3	0.3	1

The initial state of the intergranular strain tensor is determined as previously described. First, a simple example is presented to illustrate the procedure. The starting point is the fabric tensor **N**. Its components are determined from the contact normals obtained from the specimen prepared using the isotropic compression in the DEM simulation. From the fabric tensor **N** the deviatoric second order fabric tensor **F** is calculated using Equation (3):

$$\mathbf{F} = \begin{pmatrix} 0.005 & 0.008 & 0.000 \\ 0.008 & 0.005 & -0.015 \\ 0.000 & -0.015 & -0.010 \end{pmatrix}$$

The corresponding anisotropy factor a was then determined using Equation (4), as listed in Table 1. Based on this value, the weighting factor was obtained from Equation (7), with $c = 0.05$ taken in this study. This, in turn, enabled the calculation of the weighted fabric tensor **A**

$$\mathbf{A} = \begin{pmatrix} 0.580 & 0.008 & 0.000 \\ 0.004 & 0.580 & -0.008 \\ 0.000 & -0.008 & -0.572 \end{pmatrix}$$

Subsequently, the intergranular strain tensor $\boldsymbol{\delta}$ was calculated according to Equation (6), where $\boldsymbol{\delta}$ inherited its orientation from $\mathbf{A}$ and its magnitude was scaled by the hypoplastic model parameter R.

$$\boldsymbol{\delta} = \frac{\mathbf{A}}{||\mathbf{A}||} \cdot R = \begin{pmatrix} 5.780 & 0.040 & 0.000 \\ 0.040 & 5.780 & -0.080 \\ 0.000 & -0.080 & 5.720 \end{pmatrix} \cdot 10^{-5}$$

The determination of the initial intergranular strain tensors was carried out following this procedure, and the resulting tensors, including the anisotropic state, are listed in Table 3. In terms of the initially isotropic fabric, it can be observed from the example above that the determined initial intergranular strain tensor exhibits an isotropic state as well. This is expected to result in a similar stiffness response in all loading directions. In contrast, the initially anisotropic fabric shows a clear bias in the positive vertical direction for the initial intergranular strain tensor, as shown in Table 3. Consequently, when the element with the initially anisotropic state is loaded in the negative vertical direction (see Figure 2a), a higher stiffness in that direction is expected. When examining the horizontal directions (x and z), it is noticeable that both exhibit similar negative values. When the element is loaded in negative horizontal directions, a smaller stiffness in these directions is anticipated.

Table 3. Initial conditions for the element test simulations of the tests with initially isotropic and anisotropic states of the intergranular strain tensor.

State variable		isotropic	anisotropic
σ_{xx}, σ_{yy}, σ_{zz}	[kPa]	-100	
σ_{xy}, σ_{xz}, σ_{yz}	[kPa]	0	
e	[-]	0.642	0.640
δ_{xx}	[-]	$5.800 \cdot 10^{-5}$	$-4.288 \cdot 10^{-5}$
δ_{yy}	[-]	$5.800 \cdot 10^{-5}$	$8.183 \cdot 10^{-5}$
δ_{zz}	[-]	$5.720 \cdot 10^{-5}$	$-3.721 \cdot 10^{-5}$
δ_{xy}	[-]	$0.040 \cdot 10^{-5}$	$0.283 \cdot 10^{-5}$
δ_{xz}	[-]	0	$-0.567 \cdot 10^{-5}$
δ_{yz}	[-]	$-0.080 \cdot 10^{-5}$	0

Figure 7 shows the stress–strain curves obtained from the element test simulations. The element test simulations exhibit behavior qualitatively similar to that observed in the DEM simulations: The test with an initially vertically oriented intergranular strain tensor under vertical loading (A-0) reached higher deviatoric stresses earlier, while horizontal loading (A-90) results in a softer and more gradual increase. The tests with initially isotropic intergranular strains (I-0 and I-90) behaved similarly regardless of loading direction, with stress levels between those of the anisotropic cases. At about 2 % of deviatoric strain ε_q, the deviatoric stresses q of all tests converge, as the influence of the intergranular strain tensor decreases under higher strains.

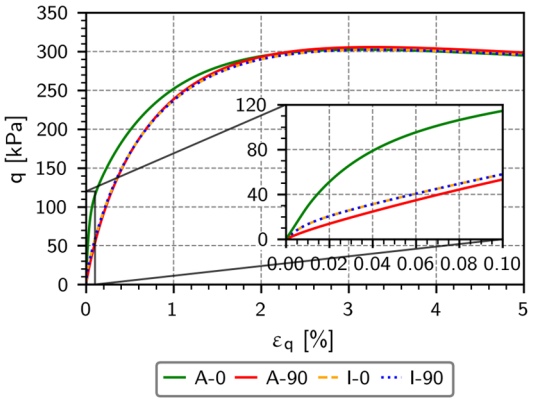

Figure 7. Element test simulations: Stress-strain curves of the tests with different initial intergranular strain tensors and loading conditions. Vertically oriented intergranular strain tensor under vertical (A-0) and horizontal (A-90) loading. Isotropic oriented intergranular strain tensor under vertical (I-0) and horizontal (I-90) loading.

Figure 8 depicts the volumetric behavior curves from the element test simulations. The differences in contractancy at small deviatoric strains (<1 %) and the subsequent transition to dilatancy originate from the influence of the initial intergranular strains and the loading direction. For the tests with the vertically oriented initial intergranular strain tensor under vertical loading (A-0), lower contractancy at small deviatoric strains (<1 %) and an earlier transition to dilatancy are observed. This behavior can be attributed to the higher stress state reached at an earlier stage (see Figure 7), which suppresses the contractive response. When loaded horizontally (A-90), small deviatoric strains (<1 %) result in a higher contractancy and a delayed transition to dilatancy. The test with an isotropic initial intergranular strain tensor shows the behavior similar to A-90, although it remains intermediate between the A-0 and A-90 responses. Since the stress states of all tests converge at approximately 2 %, the change in dilatancy diminishes, resulting in the curves running parallel thereafter.

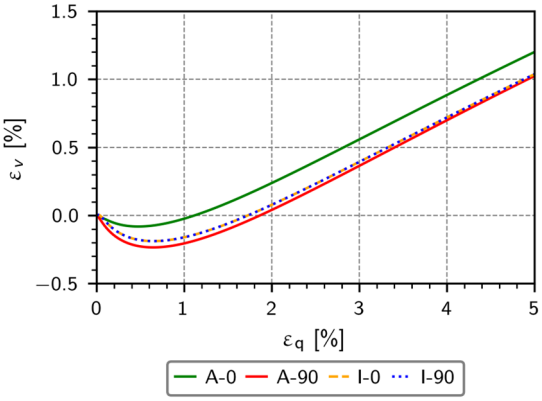

Figure 8. Element test simulations: Volumetric strain curves for different initial states of the intergranular strain tensor and loading conditions.

6 COMPARISON

As previously mentioned, the incremental stiffness was evaluated for different fabric configurations and loading directions using the secant stiffness, based on a small deviatoric strain increment of 0.1 % taken from the q–ε_q curves. To enable the comparison between the simulation methods, the stiffness values were normalized by the lowest value of each method, which was observed for the vertically oriented fabric or its corresponding intergranular strain under horizontal loading (A-

90). The absolute and relative values of the determined incremental stiffness are summarized in Table 4.

Table 4. Incremental stiffness values from DEM and element test simulations for different fabric configurations and loading directions.

	G (DEM)		G (Element test)	
	abs [kPa]	rel. [-]	abs [kPa]	rel. [-]
A-0	28327	2.23	114423	2.15
A-90	12707	1.00	53247	1.00
I-0	26657	2.10	57931	1.09
I-90	26203	2.06	57931	1.09

From the Table 4, it is obvious that the relative incremental stiffnesses qualitatively match well, indicating that the intergranular strain concept can be used to model the influence of the initial fabric on the incremental stiffness. It should be noted, that the hypoplastic model parameters were not calibrated to match with the spherical material used in the DEM simulations beforehand, resulting in quantitative differences between both simulations methods. It is therefore difficult to judge, if a higher relative stiffness of the isotropic fabric in the DEM simulations is due to the material parameters or due to the fabric effects.

In addition to the incremental stiffness, the stress–strain curves provide further insight into the influence of the initial fabric in the DEM simulations and the corresponding intergranular strain tensor in the element tests. In the DEM results, the influence of the initial fabric is evident up to approximately 8 % deviatoric strain. In contrast, the influence of the initial intergranular strain tensor diminishes earlier at 2 % deviatoric strain in the element tests, due to the limited strain range in which the intergranular strain tensor affects the hypoplastic model.

The influence of the initial fabric and the intergranular strains can also be seen in the volumetric behavior of the specimens. Both simulation methods show qualitatively consistent trends. The transition from contraction to dilatancy occurs earlier when the fabric or the corresponding intergranular strains are vertically oriented and loaded in the same direction (A-0), and are delayed under horizontal loading (A-90).

7 CONCLUSION

This study demonstrated a link between the contact fabric tensor, defined from the contact normals, and the intergranular strain tensor. In particular, a weighted fabric tensor **A** is proposed, composed of the identity tensor **I** and the deviatoric fabric tensor **F**, scaled according to the anisotropy factor *a*. The orientation of the intergranular strain tensor $\boldsymbol{\delta}$ is aligned with **A**, with its magnitude scaled to remain within the range defined by the constitutive model. The relative weighting of the components of **A** is described by an exponential function that includes a new material-dependent parameter *c*. The determination of this parameter will be examined in future works.

DEM was used to generate specimens with different initial fabrics. Their influence on incremental stiffness under different loading directions was evaluated. The fabric tensors obtained from the DEM were used to define the initial intergranular strain tensors applied in the element test simulations.

The mechanical responses from the element test simulations showed a good qualitative agreement with the DEM results, indicating that the intergranular strain tensor derived from the deviatoric fabric tensor **F** of the initial contact fabric can capture the influence of fabric anisotropy on the initial stiffness and volumetric behavior.

8 ACKNOWLEDGEMENTS

The research leading to the shown results is part of the project 453596084 (SFB/TRR 339) funded by the German Research Foundation (DFG). The financial support is greatly appreciated.

9 REFERENCES

Cundall, PA. and Strack, ODL. 1979. A discrete numerical model for granular assemblies. Geotechnique, 29(1), 47–65.

Gu, X., Hu, J. and Huang, M. 2017. Anisotropy of elasticity and fabric of granular soils. Granular Matter, 19, 33.

Gudehus, G. 1979. A comparison of some constitutive laws for soils under radially symmetric loading and unloading. In: Proceedings of the 3rd International Conference on Numerical Methods in Geomechanics, Aachen, 1309–1323

Kanatani, KI. 1984. Distribution of directional data and fabric tensors. International Journal of Engineering Science, 22(2), 149–164.

Niemunis, A. and Herle, I. 1997. Hypoplastic model for cohesionless soils with elastic strain range. Mechanics of Cohesive-frictional Materials, 2(4), 279–299.

Oda, M. 1972. Initial Fabrics and their Relations to Mechanical Properties of Granular Material. Soils and Foundations, 12(1), 17–36.

Pinzón, G., Andò, E., Desrues, J., et al. 2023. Fabric evolution and strain localisation in inherently anisotropic specimens of anisometric particles (lentils) under triaxial compression. Granular Matter, 25, 15.

Roddeman, D. 2022. Tochnog Professional User's Manual. Version 14-02-2022

Smilauer, V., Angelidakis, V., Catalano, E., et al. 2021. Yade documentation (3rd edition). Zenodo

Stamati, O., Andò, E., Roubin, E., et al. 2020. spam: Software for practical analysis of materials. Journal of Open Source Software, 5(51), 2286.

von Wolffersdorff, PA. 1996. A hypoplastic relation for granular materials with a predefined limit state surface. Mechanics of Cohesive-frictional Materials, 1(3), 251–271.